Magnetoelectric properties of 500-nm Cr_2O_3 films

P. Borisov,[1,*] T. Ashida,[2] T. Nozaki,[2] M. Sahashi,[2] and D. Lederman[1,3]

[1]*Department of Physics and Astronomy, West Virginia University, Morgantown, West Virginia 26506-6315, USA*

[2]*Department of Electronic Engineering, Tohoku University, Sendai 980-0845, Japan*

[3]*Department of Physics, University of California, Santa Cruz, California 95064, USA*

(Received 21 February 2016; revised manuscript received 13 April 2016; published 18 May 2016)

The linear magnetoelectric effect was measured in 500-nm Cr_2O_3 films grown by radio frequency sputtering on Al_2O_3 substrates between top and bottom thin film Pt electrodes. Magnetoelectric susceptibility was measured directly by applying an alternating current (ac) electric field and measuring the induced ac magnetic moment using superconducting quantum interference device magnetometry. A linear dependence of the induced ac magnetic moment on the ac electric field amplitude was found. The temperature dependence of the magnetoelectric susceptibility agreed qualitatively and quantitatively with prior measurements of bulk single crystals, but the characteristic temperatures of the film were lower than those of single crystals. It was also possible to reverse the sign of the magnetoelectric susceptibility by reversing the sign of the magnetic field applied during cooling through the Néel temperature. A competition between total magnetoelectric and Zeeman energies is proposed to explain the difference between film and bulk Cr_2O_3 regarding the cooling field dependence of the magnetoelectric effect.

DOI: 10.1103/PhysRevB.93.174415

I. INTRODUCTION

Chromium oxide (Cr_2O_3) has been intensively studied during the last 10 years because it is possible to modulate the exchange bias effect in heterostructures using electric fields [1–16]. In the antiferromagnetic (AF) state of Cr_2O_3, an applied electric field induces the magnetization, while an external magnetic field induces the dielectric polarization. The same magnetic symmetry that allows the linear magnetoelectric (ME) effect in Cr_2O_3 enables the existence of the uncompensated magnetization at the Cr_2O_3 (0001) surface, which is insensitive to the roughness [5,17]. The ME effect can be used to modify the AF domain structure and to switch between two types of 180° AF domains [18]. By modulating the interfacial magnetic moment in Cr_2O_3, it is possible to control the magnetization in an adjacent exchange coupled ferromagnetic (FM) layer [1,3]. That is, a spin valve device can be built [2,4] that allows for magnetic bit writing via the applied electric field.

The relatively small ME response of Cr_2O_3 makes its detection a complicated task, particularly in thin films; hence, Cr_2O_3 can also be considered a prototype material to test experimental approaches and techniques for measurements of the ME effect in thin film systems.

The ME effect in Cr_2O_3 has been measured previously in bulk single crystal samples [19,20]. Prior to the measurements, a single domain state was created via so-called ME field cooling (FC), where both electric (E_{fc}) and magnetic (H_{fc}) fields were applied by FC the sample from a temperature above the Néel point, $T_N = 308.5$ K. Two types of 180° AF domains can be formed in Cr_2O_3, with the spins aligned along [0001] Cr_2O_3. The ME susceptibility of the domains is defined as $\alpha = \mu_0 M/E$, where M and E denote the induced magnetization and the applied electric field, respectively, and μ_0 is the permeability of free space. In Cr_2O_3, the ME susceptibilities of the two domains have the same magnitude but opposite signs. Therefore, during the ME FC procedure, the two domains have increased or lowered total ME energy $\alpha E_{fc} H_{fc}$, depending on the sign of α, so only one domain type is formed if a large enough $E_{fc}H_{fc}$ product is realized. In particular, the sign of the single domain ME susceptibility α can be reversed if two subsequent ME FC procedures are performed in the same magnetic FC field H_{fc} but in oppositely directed electric FC fields $\pm E_{fc}$.

In this paper, we show that the ME response of 500-nm films of Cr_2O_3 correlates with the boundary magnetization in Cr_2O_3 and that the sign of the ME susceptibility can be switched completely via cooling the sample in magnetic fields of opposite directions while maintaining the electric zero field $E_{fc} = 0$. This ability to switch the sign of α is a consequence of the reduced Cr_2O_3 thickness, where the total Zeeman energy associated with the surface magnetization in Cr_2O_3 becomes comparable to the total ME energy associated with the crystal volume. This conclusion explains previous results [8,11–13] of the electric switching of the exchange bias field in all thin film systems (0001) $Cr_2O_3/[Co/Pt]_n$, where it was found that much higher field products $E_{fc}H_{fc}$ are required to achieve the switching compared to bulk single crystals of Cr_2O_3.

II. EXPERIMENT

The Cr_2O_3 films were grown by reactive radio frequency (rf) sputtering on (0001) Al_2O_3 substrates using a metal Cr target in an $Ar + O_2$ atmosphere at a substrate temperature of 773 K (base pressure $<1\times10^{-6}$ Pa). Bottom and top Pt electrodes with thicknesses of 25 nm were sputtered on Al_2O_3 substrates and Cr_2O_3 films, respectively, using shadow masking (see inset to Fig. 3). ME susceptibilities were calculated using the following sample dimensions: electrode surface areas of 10.3 and 9.5 mm^2 (relative error of ∼15%) and sample thicknesses of 0.5 mm and 500 nm for Cr_2O_3 single crystal and film samples, respectively. Electrical contacts were made using copper wires and silver paint.

*Corresponding author: pavel.borisov@mail.wvu.edu

Structural properties were studied by x-ray diffraction (XRD). The XRD scans were performed in two modes: standard ω-2θ Bragg geometry (out-of-plane scan) using D8 Advance (Bruker AXS) and horizontal (in-plane) ϕ-$2\theta_\chi$ geometry using the ATX-G setup from Rigaku. Cu K_α x-ray sources were used in both cases. In addition, cross-sectional transmission electron microscopy (TEM) was performed using the H-9000NAR setup from Hitachi High Technologies.

The total thickness of the films has been determined using a probe-type step profiler and double-checked by cross-sectional TEM on a 250-nm Cr_2O_3 film. We found a maximal 5% deviation of the total film thickness value from the nominal one.

A commercial magnetometer setup (MPMS from Quantum Design) equipped with a superconducting quantum interference device (SQUID) sensor was used for magnetic and ME measurements. The latter were performed by measuring the alternating current (ac) magnetic moment amplitudes m' and m'', $m = m'\cos(2\pi f t) + m''\sin(2\pi f t)$, excited by an applied ac electric field, $E = E_{\max}\cos(2\pi f t)$, where the frequency was chosen as $f = 17$ Hz. For more details about this technique, see [21]. The ME response was associated with m' only, while $m'' = 0$ was within error bars, as expected for low frequency ME measurements in bulk Cr_2O_3 [21]. Simultaneous application of magnetic (up to 70 kOe) and electric (up to 200 V) direct current (dc) fields was also possible. Electrical contacts were chosen such that positive electric and magnetic fields pointed in the same direction as positive magnetic moments. The first E-field half-period cycle was positive in the time dependence.

Magnetic measurements were performed using a standard sample holder. Thermoremanent magnetization (TRM) was measured under zero-field conditions upon warming the sample from 5 K to 320 K after FC from 320 K to 5 K in a magnetic field applied along the [0001] Cr_2O_3, that is, out of plane and along the spin easy axis. Averaged Al_2O_3 substrate-related magnetic remanence was calculated for temperatures >310 K (maximum of $\sim 2\times10^{-7}$ emu) and then subtracted from experimental data to make the Cr_2O_3-related phase transitions more visible.

III. RESULTS AND DISCUSSION

Figure 1(a) shows the XRD ω-2θ (out of plane) scan for the (0001) Al_2O_3/Pt 25/Cr_2O_3 500 (nm) sample. A comparison with the same scan on a (0001) Al_2O_3/Pt 25 (nm) sample without the Cr_2O_3 layer demonstrates that the (111) and (222) reflections from (111) Pt bottom electrode overlap with the (0006) and (00$\underline{12}$) reflections from (0001) Cr_2O_3. The expected film thickness effect on the XRD peak intensities is mostly compensated by the weaker coherent x-ray scattering amplitudes of (0001) Cr_2O_3 reflections with respect to (111) Pt ones. No other oxide phases (for example, CrO_2 or CrO_3) or alternative Cr_2O_3 orientations were observed. In order to verify the in-plane and out-of-plane orientation of the Cr_2O_3 film, horizontal XRD scans were performed with the scattering vector q corresponding to the Al_2O_3 (10-10) (green line) and (11-20) (red line) [Fig. 1(b)] Al_2O_3 substrate planes on the (0001) Al_2O_3/Pt 25/Cr_2O_3 500 (nm) sample. The results confirm the (0001) orientation of the Cr_2O_3 layer, with the corresponding in-plane orientation Al_2O_3 [10-10] $\|$ Cr_2O_3 [10-10], though we observed a weak Cr_2O_3 peak for Al_2O_3 [11-20] $\|$ Cr_2O_3 [10-10]; i.e., Cr_2O_3 rotated in plane by 30° with respect to Al_2O_3. The latter alternative in-plane orientation was more pronounced in thinner (20 nm) Cr_2O_3 films grown on (0001) Al_2O_3/(111) Pt [16]; hence, this feature seems to be related to crystallographic defects due to the interface (111) Pt/(0001) Cr_2O_3.

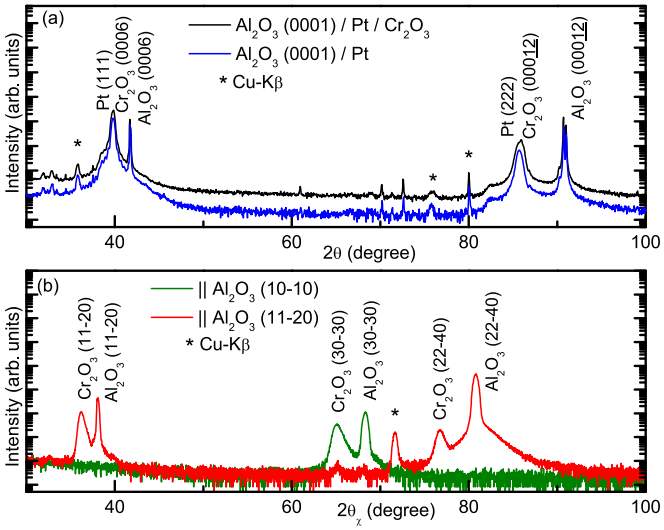

FIG. 1. XRD structural characterization: (a) XRD out-of-plane ω-2θ scan from a 500-nm Cr_2O_3 film grown on Al_2O_3 (0001)/Pt 25-nm substrate (black line). For comparison, the XRD pattern from Al_2O_3 (0001)/Pt 25 nm is shown (blue line). Cr_2O_3 (000l) peaks overlap with Pt (111) and (222) reflections. (b) XRD ϕ-$2\theta_\chi$ in-plane scan for the Al_2O_3/Pt 25/Cr_2O_3 500 (nm) sample along Al_2O_3 (10-10) (green line) and (11-20) (red line) planes. The corresponding azimuthal (ϕ) angle was adjusted in order to observe different crystallographic planes.

Since no reflections from Pt bottom electrodes were observed in ϕ-$2\theta_\chi$ (in-plane) scans, due to the small probing depth and relatively thick Cr_2O_3 layer, we repeated the same scans for (0001) Al_2O_3/Pt 25 (nm) samples and found Pt {2-20} peaks (not shown) for both cases of q probing crystal planes parallel to Al_2O_3 (10-10) or Al_2O_3 (11-20).

The cross-sectional TEM image shown in Fig. 2 confirms crystalline (0001) Cr_2O_3 quality, while the Pt bottom electrode shows different in-plane structural domains. In conclusion, the structural studies verified single crystalline quality of the Cr_2O_3 films. Similar-quality films have been used to demonstrate successful electric switching of the exchange bias field associated with the heterostructures Al_2O_3 (0001)/Pt/Cr_2O_3 (0001)/Pt/Co/Pt [8,13].

Figure 3 shows ac magnetic moment amplitude m' vs E-field amplitude $E_{\max}$ measured at 250 K. In order to prepare a single AF domain state, the sample was cooled down in $H_{fc} = 10$ kOe, as discussed below. A linear dependence was found, confirming that the ME effect in 500-nm Cr_2O_3 is qualitatively similar to the one in the bulk Cr_2O_3. Here, $m' = (V/\mu_0)\alpha E_{\max}$, where V is the Cr_2O_3 volume. The absolute value of the corresponding ME susceptibility was calculated from the slope, $\alpha = 4.6 \pm 0.3$ ps m^{-1}. ME measurements on another Cr_2O_3 film sample grown and field cooled under

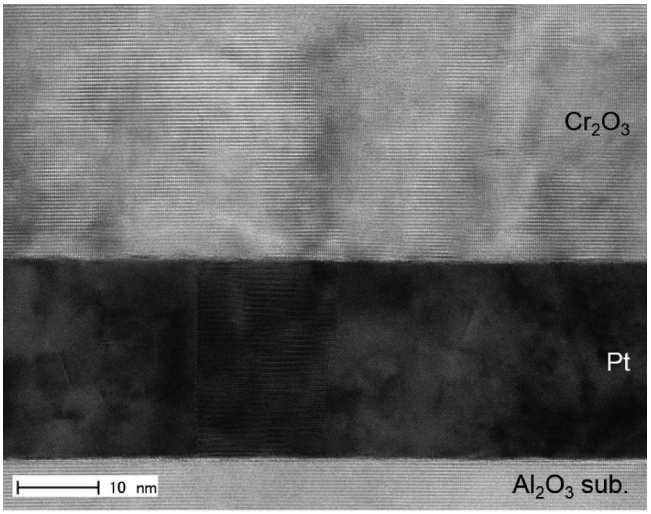

FIG. 2. Cross-sectional TEM image on (0001) Al_2O_3/Pt 25/Cr_2O_3 250 (nm). The discontinuous pattern on the Pt layer indicates its texture.

identical conditions yielded $\alpha = 4.1 \pm 0.3\,\mathrm{ps\,m^{-1}}$, that is, our results were reproducible between films from the same batch. Also, the absolute values of the ME susceptibility for the film samples are in agreement with the single crystal data, as discussed below.

The temperature dependence of the ME susceptibility $\alpha = \mu_0 m'/(V E_{\max})$ is shown in Fig. 4. The film was cooled from 320 K to 100 K in magnetic fields 1 or 10 kOe and then measured while warming from 5 K. $E_{\max}$ values were adjusted in different temperature ranges in order to achieve a compromise between a low leakage current and a large signal magnitude. Note the thermal activation character of the electrical conductivity in Cr_2O_3 [22]. Typical ac field amplitude values were $62.4\,\mathrm{kV\,cm^{-1}}$ between 5 K and 95 K (maximal

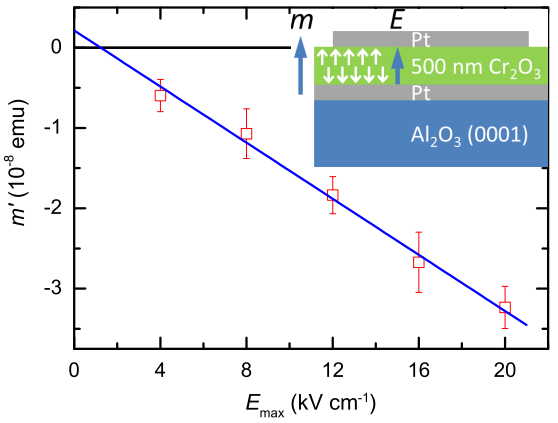

FIG. 3. The ac magnetic moment amplitude m' vs ac electric field amplitude $E_{\max}$ measured on 500-nm Cr_2O_3 film at 250 K after cooling from 310 K in a 10-kOe magnetic field. The blue solid line is the corresponding linear fit. The slope obtained from the fit is proportional to the linear ME susceptibility. Top right inset: illustration of the thin film cross-section structure, together with magnetic moment ($\boldsymbol{m}$), electric field ($\boldsymbol{E}$), and Cr^{3+} spin vectors orientations.

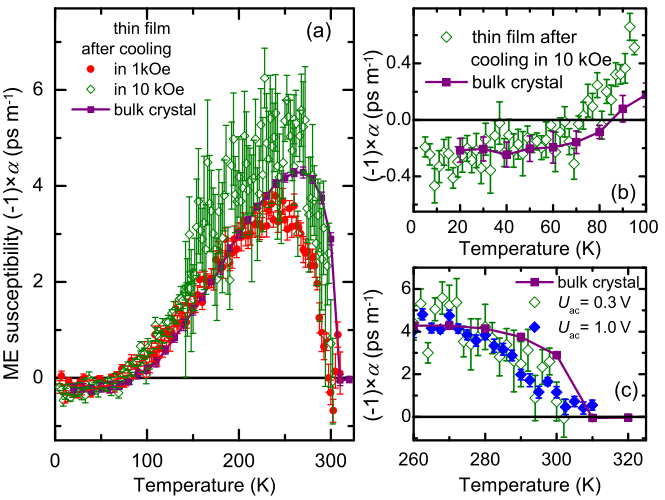

FIG. 4. ME susceptibility α vs temperature. (a) Comparison between a 500-nm Cr_2O_3 film and a thick single crystal (0.5 mm) of Cr_2O_3. The film was either cooled from 320 K to 100 K in 1 kOe and measured using ac electric field amplitudes of $62.4\,\mathrm{kV\,cm^{-1}}$ (between 5 K and 95 K), $31.2\,\mathrm{kV\,cm^{-1}}$ (between 97 K and 151 K), and $20\,\mathrm{kV\,cm^{-1}}$ (between 152.5 K and 310 K) or field cooled in 10 kOe and then measured using ac electric field amplitudes $62.4\,\mathrm{kV\,cm^{-1}}$ (between 5 K and 95 K), $31.2\,\mathrm{kV\,cm^{-1}}$ (between 95 K and 151 K), and $6.24\,\mathrm{kV\,cm^{-1}}$ (between 142 K and 302 K). The thick single crystal was ME cooled from 320 K to 260 K in 30 kOe and $1\,\mathrm{kV\,cm^{-1}}$. (b) Low temperature data from (a) for film cooled in 10 kOe and for bulk single crystal. (c) High temperature data for bulk single crystal in (a) and for film cooled in 10 kOe and then measured either using $6.24\,\mathrm{kV\,cm^{-1}}$ (i.e., $U_{ac} = 0.31$ V) or $20\,\mathrm{kV\,cm^{-1}}$ (i.e., $U_{ac} = 1.0$ V) ac field amplitudes. In all figures, experimental data points for α were multiplied by (-1) for better representation.

leakage currents $i_{\max} < 10\,\mathrm{nA}$), $31.2\,\mathrm{kV\,cm^{-1}}$ between 97 K and 150 K ($i_{\max} < 10\,\mathrm{nA}$), and $6.24\,\mathrm{kV\,cm^{-1}}$ ($i_{\max} < 300\,\mathrm{nA}$) or $20\,\mathrm{kV\,cm^{-1}}$ ($i_{\max} < 3\,\mu\mathrm{A}$) at temperatures above 150 K. The largest measurement temperature was limited to 310 K in order to minimize the risk of a dielectric breakdown in the film.

Figure 4(a) shows a comparison of the ME susceptibilities of the film and bulk single crystal samples. The error bars refer to statistical uncertainties determined from the standard error of the average of multiple measurements. The single crystal was cooled in $H_{\mathrm{fc}} = 30\,\mathrm{kOe}$ and $E_{\mathrm{fc}} = 1\,\mathrm{kV\,cm^{-1}}$. Prior to the measurements, the film sample was cooled in a magnetic field only. The largest ME response was found after FC in $H_{\mathrm{fc}} \geqslant 10\,\mathrm{kOe}$, with the magnitude of ME susceptibility α being comparable to the bulk single crystal values. The film cooled in a smaller $H_{\mathrm{fc}} = 1\,\mathrm{kOe}$ showed a decrease in $|\alpha|$ of 30%, most likely because the cooling field was not strong enough to align the complete Cr_2O_3 surface in a single direction. This caused the two 180° AF domains to form with opposite signs of α. This explanation assumes that the relative distribution of the AF domains is controlled by the boundary magnetization distribution. The results of dc magnetic measurements discussed below support this hypothesis.

In the film sample, ME susceptibility α shows a sign reversal at low temperatures ~70 K [Fig. 4(b)] and a maximum

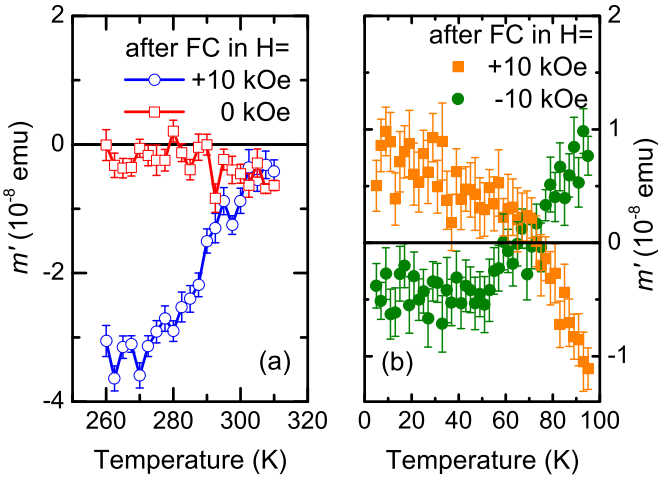

FIG. 5. Electrically induced magnetic ac moment amplitude m' vs temperature measured under different FC protocols on a 500-nm Cr_2O_3 film. (a) Measurements in the 260 K to 310 K temperature range with an electric field ac amplitude of 20 kV cm^{-1}. (b) Measurements in the 5K to 95K temperature range with an electric field ac amplitude of 62.4 kV cm^{-1}.

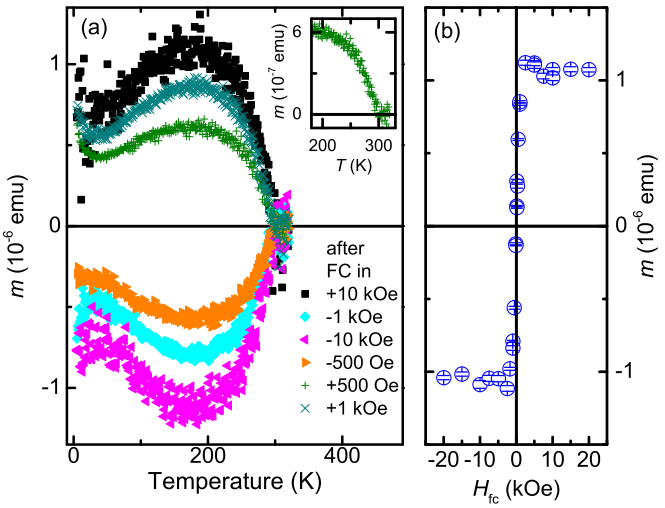

FIG. 6. TRM measured after FC from 320 K to 5 K in different values of H_{fc}. (a) TRM magnetic moment m_{TRM} vs temperature. The fields are listed from the top in the same sequences applied in the experiment. Inset: enhanced view for $H_{fc} = 500$ Oe. (b) Magnetic moment m_{TRM} vs H_{fc} averaged for temperatures between 195 K and 205 K.

below room temperature ~250 K [Fig. 4(a)], with the signal disappearing above ~300 K, that is, above T_N [Fig. 4(c)] (film data were measured with different ac amplitudes, 6.24 or 20.0 kV cm^{-1}, hence the different relative errors in α). These results are similar to what was observed in the bulk crystal sample (Fig. 4). As discussed below, we were also able to identify T_N of ~300 K from dc magnetic measurements on films (as will be shown in Fig. 6). Due to the difference in T_N values between the film and the bulk single crystal samples, the relevant temperatures are also lower in the case of the films; cf. the response at 80 K, 260 K, and 310 K in the case of a single crystal. A relatively unlikely scenario of the weak dc moment in Cr_2O_3 being somehow coupled to the ME ac susceptibility response can be excluded, since the sign reversal was found ~70 K in the ME response [Fig. 4(b)] but was not observed in the dc magnetization measurements (see Fig. 6).

The magnetic field applied during FC played the predominant role in the outcome of the ME measurements in films. Cooling in $H_{fc} = 0$ resulted in the absence of a ME response [Fig. 5(a)], while subsequent cooling in two fields of the same magnitude but applied in opposite directions switched the sign of α [Fig. 5(b)]. That is, the boundary magnetization couples directly to the external magnetic field and allows AF domain reversal [9].

We attempted to achieve true ME switching of α by applying the same H_{fc} and reversing the direction of E_{fc} applied during ME cooling from 310 K, but no switching was found using this procedure. The largest field product of $|H_{fc}| = 50$ kOe and $|E_{fc}| = 60$ kV cm^{-1} was not successful, while the films were destroyed for $E_{fc} \geqslant 80$ kV cm^{-1} due to a dielectric breakdown. The lower breakdown field value when compared to previous reports [8,11–13] is likely due to the larger electrode size in our case.

The results of the dc magnetic measurements are shown in Fig. 6. The remanent magnetic moment peaks ~200 K and disappears above T_C of ~300 K, which agrees well with the critical temperature identified from the ME measurements [Fig. 4(c)], that is, with T_N. The temperature dependence is similar to prior results from thinner (26–60 nm) Cr_2O_3 films [9,14]. In thinner films, it has been demonstrated that the uncompensated magnetic moment originates from the boundary magnetization coupled to the AF order parameter and is insensitive to the surface roughness [5,17,23]. The largest magnetic remanence occurred in the temperature interval between 195 K and 205 K. The magnetic moment was saturated for $H_{fc} \geqslant 2.5$ kOe [Fig. 6(b)]. Prior papers by Fallarino *et al.* [9,14] considered the isothermal switching of the AF domain state in Cr_2O_3 films at $T < T_N$ in $H_{fc} \geqslant 10$ kOe and found that the corresponding temperature at which the isothermal switching occurs, T_f, scales as $T_f = T_N - H_{fc}^2/b$, i.e., $T_f < T_N$. By using the parameter b from [14] for 60 nm Cr_2O_3, as well as $T_N = 300$ K and $H_{fc} = 2.5$ kOe, we obtain $T_f = 299.99$ K $\approx T_N$; that is, the Zeeman energy-induced AF state reversal via FC in $H_{fc} = 2.5$ kOe is likely not distinguishable from an isothermal effect.

As in Ref. [5], we recalculate the absolute value of the uncompensated moment associated with the boundary magnetization in Cr_2O_3 films (Fig. 6) into moment per hexagonal unit cell area, 64 Å^2, of the (0001) Cr_2O_3 film surface (total area of 16.3 mm^2). Using the maximum observed saturation moment of $\sim 1.1 \times 10^{-6}$ emu, we obtain 4.7μ_B per unit cell area, which is close to the 5.6μ_B obtained for prior measurements of a 200-nm Cr_2O_3 film and explained by two Cr^{3+} spin moments of 3μ_B (theoretical value) located in each hexagonal unit area [5]. However, this conclusion depends on the (0001) surface termination and spin structure. Assuming the (0001) Cr_2O_3 surface terminates as a half-cut through the Cr^{3+} buckled layer between two adjacent closed-packed oxygen layers, as shown in Fig. 7 and in agreement with the literature [24–26], we calculate one Cr^{3+} spin per hexagonal unit area of a single surface, or two spins in total, if top

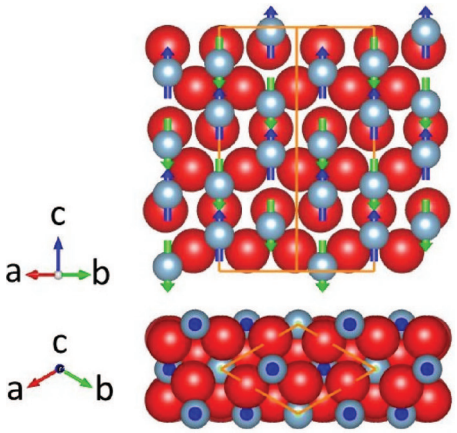

FIG. 7. Top: sketch of the (11-20) Cr_2O_3 surface. Bottom: sketch of the (0001) Cr_2O_3 surface. Large red and small gray spheres represent O^{2-} and Cr^{3+} ions, respectively. Up and down arrows denote magnetic Cr^{3+} moments oriented according to the AF spin order in bulk Cr_2O_3. Unit cell projections are drawn with thick orange lines. The spin structure shown represents one of two 180° AF domains, labeled type B and corresponding to a negative ME susceptibility at $T > 80$ K and to a positive top boundary magnetization along the [0001] axis. A half-cut through the buckled plane of Cr^{3+} ions between two adjacent oxygen layers is taken as a (0001) surface termination.

and bottom surfaces are considered. Alternatively, one can consider a complete oxygen layer at the bottom surface and a complete buckled Cr^{3+} layer located on the top surface above the oxygen layer. In both cases, some surface spins would have to be oriented along H_{fc}, that is, reversed with respect to the bulk structure, in order to yield a nonzero magnetic moment in total. The representation of the magnetic moments shown in Fig. 7 is an idealization. Surface magnetization in (0001) Cr_2O_3 has been verified both experimentally and theoretically in Ref. [23], but the exact relationship between surface and bulk spins is still unclear. The observed 19% discrepancy between our result, $4.7\mu_B$ per hexagonal unit cell area, and the moment found in Ref. [5], $5.7\mu_B$, could be explained by the 15% relative error in our electrode area estimation.

Prior papers [18–20] about the ME properties of Cr_2O_3 single crystals reported that the 180° AF domain type can be selected by applying E_{fc} and H_{fc} parallel or antiparallel to each other and to the [0001] c axis during ME FC. In the discussion below, we assume that the magnetic field direction is always positive and applied along the c axis. However, the same literature reported that H_{fc} applied by itself during FC had some effect on the sign of the resulting ME susceptibility [18–20]. The origin of the effect was not clear, since both types of AF domains should have the same magnetic susceptibility. Astrov [19] found that $H_{fc} = 500$ Oe was enough to reverse the sign of the ME susceptibility in single crystals. A weak negative ME response at $T = 150$ K was obtained for single crystals (0001) Cr_2O_3 in Ref. [3] after a purely magnetic FC in a positive $H_{fc} = 5$ kOe. Analysis of the spin structures in Cr_2O_3 using spherical neutron polarimetry [27–29] demonstrated that ME cooling in antiparallel $\boldsymbol{E}_{fc}$ and $\boldsymbol{H}_{fc}$ yields the AF domain type with the positive top magnetization, as shown in Fig. 7. We propose to call this a B-type AF domain, distinguished from an A-type domain by 180° rotation of all spins. The surface magnetization of a Cr_2O_3 single crystal prepared by ME cooling in parallel $\boldsymbol{E}_{fc}$ and $\boldsymbol{H}_{fc}$ was analyzed in Ref. [5] using spin-polarized photoemission spectroscopy results, and an opposite, that is, negative surface magnetization, was obtained for this A-type domain. Furthermore, by analyzing the ME results from the literature [3,30,31] we assign a positive and a negative α for the temperature region >80 K to domain types A and B, respectively. That is, our experimental results of $\alpha < 0$ at $T > 80$ K after FC in positive magnetic fields can be explained by the formation of the B-type domain with the positive top boundary magnetization aligned parallel to $\boldsymbol{H}_{fc}$.

The failure to achieve an AF single domain reversal via the ME FC procedure can be explained by the fact that with the reduced thickness of Cr_2O_3 single crystal film, the Zeeman energy $\mu_0 m_S H_{fc}$, associated with the surface magnetic moment m_S, becomes comparable to the total ME energy $\alpha E_{fc} H_{fc} V$, associated with the total volume V. Thus, purely magnetic switching via $\mu_0 m_S H_{fc}$ competes with ME switching via the $\alpha E_{fc} H_{fc} V$ energy term when the corresponding energy terms promote the growth of the single domain type B and A, respectively. In order to estimate the corresponding energies of our samples, $T = 297.5$ K was chosen as the relevant temperature, being relatively close to T_N but, at the same time, where the corresponding ME susceptibility was measured with sufficient precision, $\alpha = 1.7 \pm 0.2$ ps m^{-1}, after FC in 10 kOe [Fig. 5(a)]. The corresponding dc moment at $T = 297.5$ K was obtained via interpolation of TRM m_{dc} vs T data [Fig. 6(a)] for 2.5 kOe $\leqslant |H_{dc}| \leqslant$ 10 kOe and 260 K $\leqslant T \leqslant$ 305 K using $m_{dc} = a(T_N - T)^{\beta}$, where $T_N = 300$ K, a is a fitting parameter, and $\beta = 0.8$ is the surface critical exponent [6,15]. The surface moment was fully saturated for the whole H_{dc} range [Fig. 6(b)]; therefore, we used an averaged $|m_{dc}(T = 297.5\,\text{K})| = (8.1 \pm 0.2) \times 10^{-11}$ Am^2. By substituting these values and using $H_{fc} = 50$ kOe and $E_{fc} = 60$ kV cm^{-1}, we obtained for the Zeeman and ME energies 0.40 ± 0.01 and 0.19 ± 0.02 nJ, respectively. That is, the Zeeman energy was higher under the given conditions, thus preventing switching via the ME energy from the negative towards the positive ME susceptibility α. When replacing $m_S = \sigma S$ and $V = dS$, where σ, S, and d are the surface moment density, film area, and film thickness, respectively, then the minimum E_{fc} required to achieve ME switching is

$$E_{fc} > \mu_0 \sigma / (\alpha d), \tag{1}$$

or $E_{fc} > 130 \pm 16$ kV cm^{-1} if the above parameters are used. This value is higher than the $E_{fc} = 60$ kV cm^{-1} that we could apply in our experiments without destroying the sample.

Interestingly, it has already been found that the exchange bias systems made from (0001) Cr_2O_3 films (150–250 nm) require higher field products $E_{fc} H_{fc}$ to achieve AF single domain switching via ME FC [8,11–13]. In those systems, the AF single domain type is responsible for the switching of the FM hysteresis bias, characterized via the so-called exchange bias field H_{EB}. The microscopic origin is the exchange interaction at the FM-AF interface. Toyoki *et al.* [11,12] reported, for their exchange bias systems with 150-nm Cr_2O_3, switching products $E_{fc} H_{fc} \geqslant 4212$ kOe · kV cm^{-1} and $E_{fc} H_{fc} \geqslant 6714$ kOe · kV cm^{-1} for the textured and twinned

Cr_2O_3 films, respectively. By recalculating the switching product for 150-nm instead of 500-nm thickness, we obtain $E_{fc}H_{fc} > (4318 \pm 532)\,\mathrm{kOe \cdot kV\,cm^{-1}}$; that is, our estimate is close to the experimental values if $H_{fc} = 10\,\mathrm{kOe}$ is chosen. Our results also contradict the hypothesis made in Refs. [11] and [12] to explain the increased switching field products: Cr_2O_3 films might have ME susceptibility values much lower than those in the bulk. By another comparison with the exchange bias switching experiments for exchange bias systems with 250-nm Cr_2O_3, the field switching products were reported to be 400 and $2000\,\mathrm{kOe \cdot kV\,cm^{-1}}$ in Refs. [8] and [13], whereas our estimates yield $E_{fc}H_{fc} > (2591 \pm 319)\,\mathrm{kOe \cdot kV\,cm^{-1}}$ for $d = 250\,\mathrm{nm}$ and $H_{fc} = 10\,\mathrm{kOe}$. That is, we have rather good agreement with the results in Ref. [13]. In addition, the exchange bias samples prepared for characterization via the anomalous Hall effect were patterned into areas much smaller than our samples area; cf. microdots with a 20-μm diameter or $40\times40\,\mu\mathrm{m}$ cross-point area in Refs. [11,12] and [13], respectively. This could have had an additional effect on the Cr_2O_3 ME switching characteristics. Typical lateral dimensions of AF domains in bulk (0001) Cr_2O_3 are $\geqslant 1\,\mathrm{mm}$ [32].

An additional factor that could affect the results is the possible pinning effects for AF domains, reported, for example, in bulk single crystals of Cr_2O_3 [32]. Pinning could result in an energy barrier W_b that prevents the formation of a reversed domain state upon ME FC from above T_N. Pinning sites could consist of crystallographic defects in the bulk crystal or film. Adding this energy barrier per film area, $w_b = W_b/S$, to Eq. (1) would modify it to

$$E_{fc} > \mu_0\sigma/(\alpha d) + w_b/(\alpha d) \times (1/H_{fc}). \quad (2)$$

Thus, the existence of a switching barrier would further increase the minimal E_{fc} values required for a ME switching and by extension would provide an additional functional dependence on H_{fc}. The same functional dependence was found in [11,12] for exchange bias systems with 150-nm (0001) Cr_2O_3. A comparison between twinned and textured Cr_2O_3 films in [11,12] yielded different slopes and intersection values for E_{fc} vs $1/H_{fc}$ dependences. Those differences could be then explained by a distinction between energy barriers and surface magnetization in the Cr_2O_3 films of different structural quality.

IV. SUMMARY

The ME effect was measured on 500-nm Cr_2O_3 films grown by rf sputtering between two thin film Pt electrodes on Al_2O_3 (0001) substrates. The ME response was linear with respect to the applied electric field and similar in magnitude to the response observed for bulk single crystals. The relevant temperatures in the temperature dependence of the ME susceptibility were lower than for thick single crystals of Cr_2O_3. We were able to switch the sign of the ME susceptibility by cooling in magnetic fields of opposite directions. Attempts to switch the sign of the ME susceptibility via the so-called ME FC were not successful, presumably as a result of competition between the total Zeeman energy associated with the film surface and the total ME energy associated with the film volume.

ACKNOWLEDGMENTS

This paper was supported in part by the West Virginia Higher Education Policy Commission, Research Challenge Grant No. HEPC.dsr.12.29, West Virginia University (WVU) Shared Research Facilities, and Council for Science, Technology and Innovation ImPACT program through government of Japan.

[1] A. Hochstrat, C. Binek, X. Chen, and W. Kleemann, J. Magn. Magn. Mater. **272-276**, 325 (2004).
[2] C. Binek and B. Doudin, J. Phys.: Condens. Matter **17**, L39 (2005).
[3] P. Borisov, A. Hochstrat, X. Chen, W. Kleemann, and C. Binek, Phys. Rev. Lett. **94**, 117203 (2005).
[4] X. Chen, A. Hochstrat, P. Borisov, and W. Kleemann, Appl. Phys. Lett. **89**, 202508 (2006).
[5] X. He, Y. Wang, N. Wu, A. N. Caruso, E. Vescovo, K. D. Belashchenko, P. A. Dowben, and C. Binek, Nat. Mater. **9**, 579 (2010).
[6] P. Borisov and W. Kleemann, J. Appl. Phys. **110**, 033917 (2011).
[7] T. Ashida, Y. Sato, T. Nozaki, and M. Sahashi, J. Appl. Phys. **113**, 17D711 (2013).
[8] T. Ashida, M. Oida, N. Shimomura, T. Nozaki, T. Shibata, and M. Sahashi, Appl. Phys. Lett. **104**, 152409 (2014).
[9] L. Fallarino, C. Binek, and A. Berger, Appl. Phys. Lett. **104**, 022403 (2014).
[10] T. Nozaki, M. Oida, T. Ashida, N. Shimomura, T. Shibata, and M. Sahashi, Appl. Phys. Lett. **105**, 212406 (2014).
[11] K. Toyoki, Y. Shiratsuchi, T. Nakamura, C. Mitsumata, S. Harimoto, Y. Takechi, T. Nishimura, H. Nomura, and R. Nakatani, Appl. Phys. Expr. **7**, 114201 (2014).
[12] K. Toyoki, Y. Shiratsuchi, A. Kobane, S. Harimoto, S. Onoue, H. Nomura, and R. Nakatani, J. Appl. Phys. **117**, 17D902 (2015).
[13] T. Ashida, M. Oida, N. Shimomura, T. Nozaki, T. Shibata, and M. Sahashi, Appl. Phys. Lett. **106**, 132407 (2015).
[14] L. Fallarino, A. Berger, and C. Binek, Phys. Rev. B **91**, 054414 (2015).
[15] L. Fallarino, C. Binek, and A. Berger, Phys. Rev. B **91**, 214403 (2015).
[16] S. P. Pati, N. Shimomura, T. Nozaki, T. Shibata, and M. Sahashi, J. Appl. Phys. **117**, 17D137 (2015).
[17] K. D. Belashchenko, Phys. Rev. Lett. **105**, 147204 (2010).
[18] T. J. Martin and J. C. Anderson, Phys. Lett. **11**, 109 (1964).
[19] D. N. Astrov, Sov. Phys. JETP **13**, 729 (1961).
[20] G. T. Rado and V. J. Folen, Phys. Rev. Lett. **7**, 310 (1961).
[21] P. Borisov, A. Hochstrat, V. V. Shvartsman, and W. Kleemann, Rev. Sci. Instr. **78**, 106105 (2007).
[22] C.-P. Kwan, R. Chen, U. Singisetti, and J. P. Bird, Appl. Phys. Lett. **106**, 112901 (2015).

[23] N. Wu, X. He, A. L. Wysocki, U. Lanke, T. Komesu, K. D. Belashchenko, C. Binek, and P. A. Dowben, Phys. Rev. Lett. **106**, 087202 (2011).
[24] M. Bender, D. Ehrlich, I. N. Yakovkin, F. Rohr, M. Bäumer, H. Kuhlenbeck, H.-J. Freund, and V. Staemmler, J. Phys.: Condens. Matter **7**, 5289 (1995).
[25] T. Gloege, H. L. Meyerheim, W. Moritz, and D. Wolf, Surf. Sci. **441**, L917 (1999).
[26] O. Bikondoa, W. Moritz, X. Torrelles, H. J. Kim, G. Thornton, and R. Lindsay, Phys. Rev. B **81**, 205439 (2010).
[27] P. J. Brown, J. B. Forsyth, and F. Tasset, J. Phys.: Condens. Matter **10**, 663 (1998).
[28] P. J. Brown, J. B. Forsyth, E. Lelievre-Berna, and F. Tasset, J. Phys.: Condens. Matter **14**, 1957 (2002).
[29] P. J. Brown, J. B. Forsyth, and F. Tasset, Solid State Sci. **7**, 682 (2005).
[30] T. H. O'Dell, Philos. Mag. **13**, 921 (1966).
[31] A. Malashevich, S. Coh, I. Souza, and D. Vanderbilt, Phys. Rev. B **86**, 094430 (2012).
[32] M. Fiebig, D. Fröhlich, G. Sluyterman v. L., and R. V. Pisarev, Appl. Phys. Lett. **66**, 2906 (1995).